Acceleration of cosmic rays on the forward and reverse shocks in supernova remnants

V.N.Zirakashvili, V.S.Ptuskin

Pushkov Institute of Terrestrial Magnetism, Ionosphere and Radiowave Propagation, Russian Academy of Sciences (IZMIRAN), 142190 Troitsk, Moscow Region, Russia

Outline

- Acceleration of particles at forward and reverse shocks in SNRs
- Amplification of magnetic fields
- Radioactivity and electron acceleration
- Modeling of DSA in SNRs

Diffusive Shock Acceleration

Krymsky 1977; Bell 1978; Axford et al.1977; Blandford & Ostriker 1978

Very attractive feature: power-law spectrum of particles accelerated, $\gamma=(\sigma+2)/(\sigma-1)$, where σ is the shock compression ratio, for strong shocks $\sigma=4$ and $\gamma=2$

Maximum energy for SN: $D \sim 0.1 u_{sh} R_{sh}$ $\sim \mathbf{3 \cdot 10^{27}}$ $cm^2/s < D_{gal}$

Diffusion coefficient should be small in the vicinity of SN shock

In the Bohm limit $D=D_B=cr_g/3$ and for interstellar magnetic field

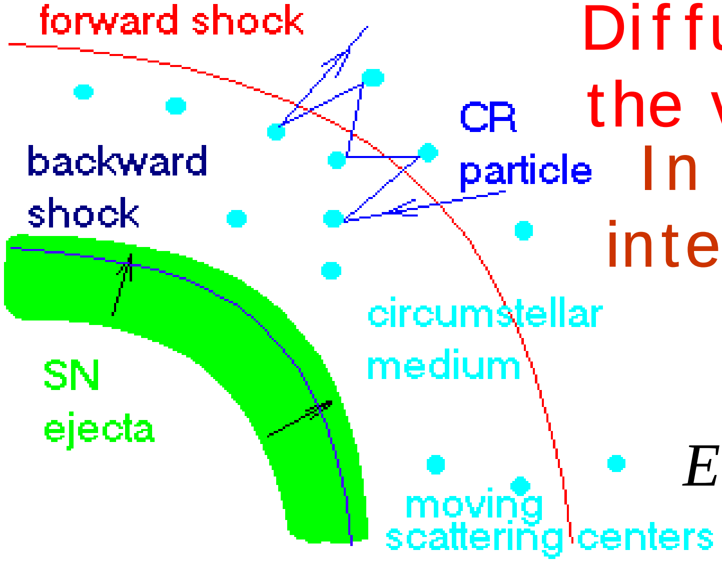

$$E_{\max} = Z \cdot 10^{14}\,\mathrm{eV} \left(\frac{B}{10\,\mu\mathrm{G}}\right)\left(\frac{R_{\mathrm{sh}}}{3\,\mathrm{pc}}\right)\left(\frac{u_{\mathrm{sh}}}{3000\ \mathrm{km\ s^{-1}}}\right)$$

Shock modification by the pressure of accelerated CRs.

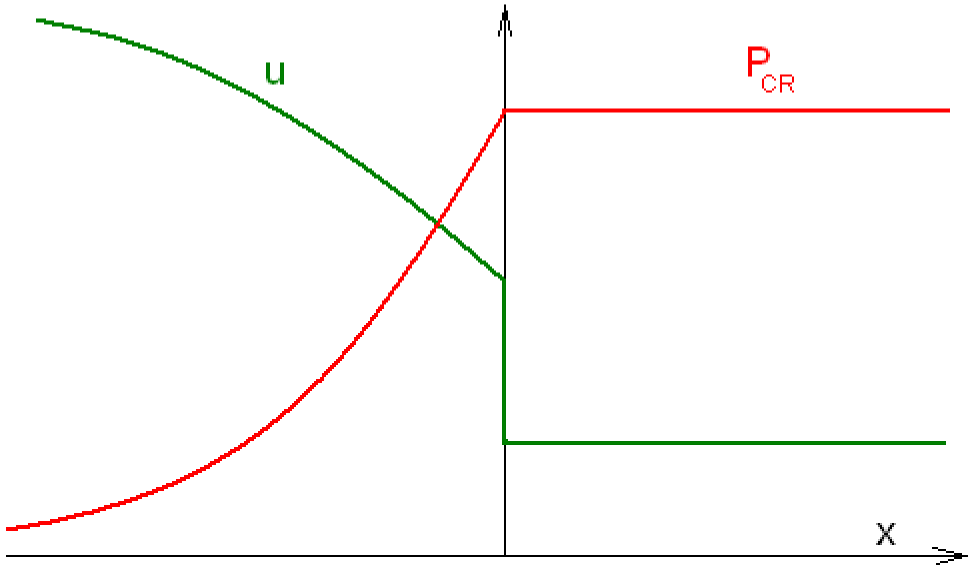

Axford 1977, 1981

Eichler 1984

Higher compression ratio of the shock, concave spectrum of particles.

X-ray image of Tycho SNR (from Warren et al. 2005)

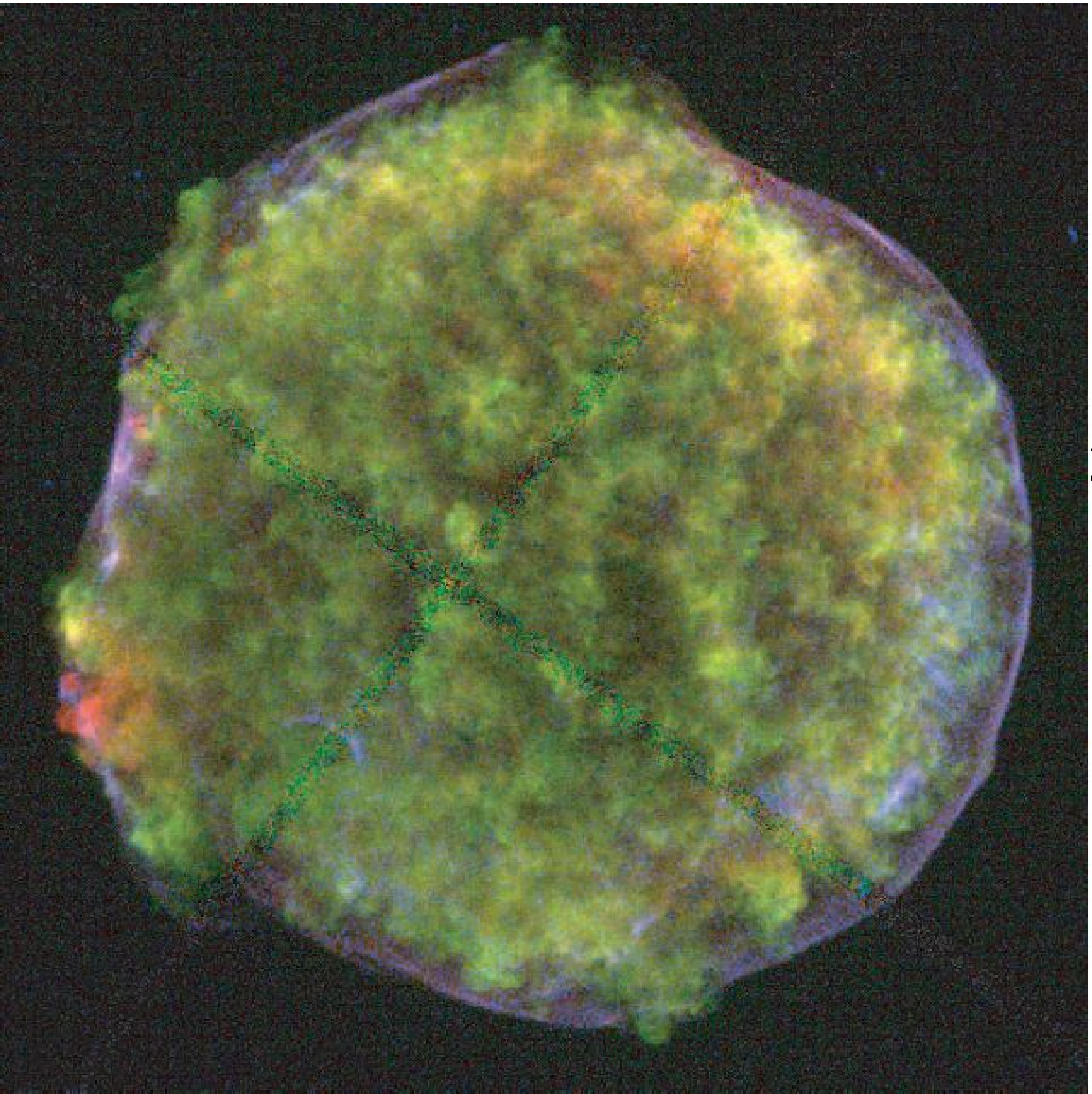

1. CD is close to the forward shock – evidence of the shock modification by CR pressure.
2. Thin non-thermal X-ray filaments at the periphery of the remnant – evidence of electron acceleration and of magnetic amplification.

Magnetic field amplification by non-resonant streaming instability

Bell (2004) used Achterberg's results (1983) and found the regime of instability that was overlooked

$$F_{CR} = -\frac{1}{c}\left[j_d \times B \right]$$

$$\omega^2 = V_a^2 k^2 - j_d \frac{B_0 k}{c \rho_0}$$

$$k\, r_g >>1, \gamma_{max}=j_d B_0/2c\rho V_a$$

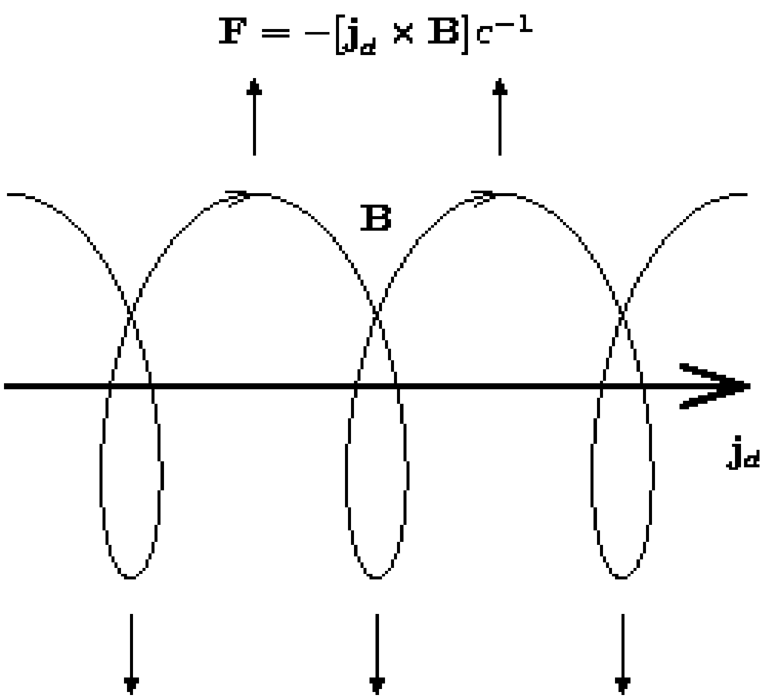

Since the CR trajectories are weakly influenced by the small-scale field, the use of the mean j_d is well justfied

saturated level of instability

$$B \approx \frac{4\pi}{ck} j_d$$

MHD modeling in the shock transition region and downstream of the shock

Zirakashvili & Ptuskin 2008

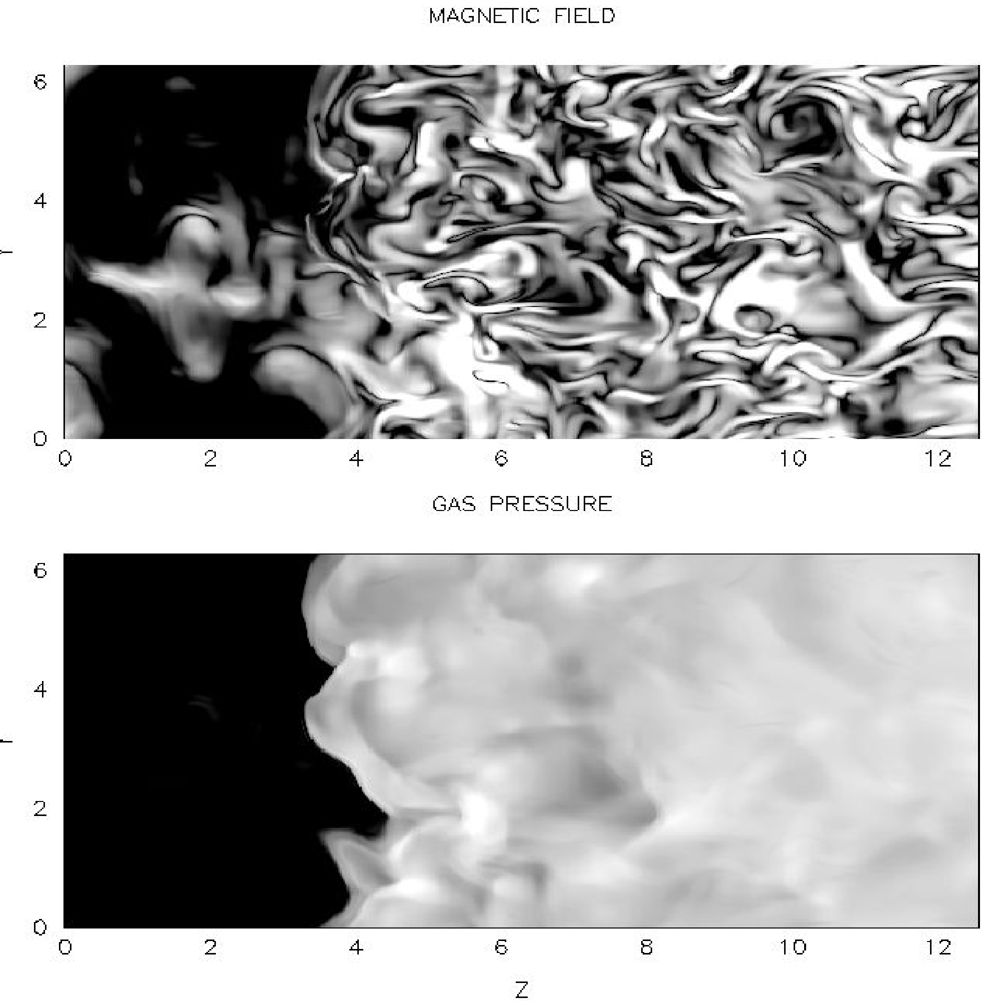

3D $256^2 \times 512$

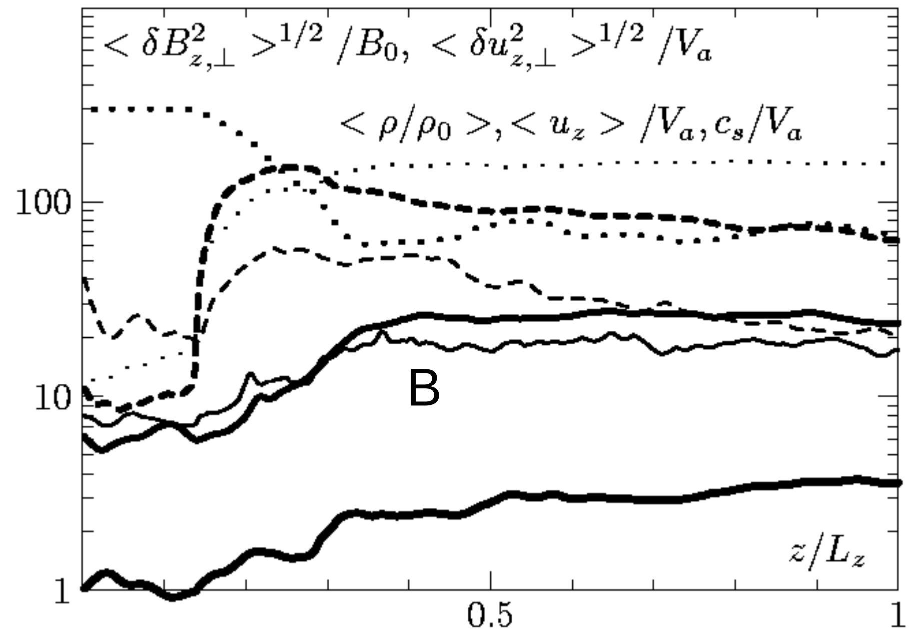

u_1=3000 km/s V_a=10 km/s

η_{esc}=0.14

0.02L

Magnetic field is not damped and is perpendicular to the shock front downstream of the shock!

Ratio=1.4 σ_B=3

Wood & Mufson 1992

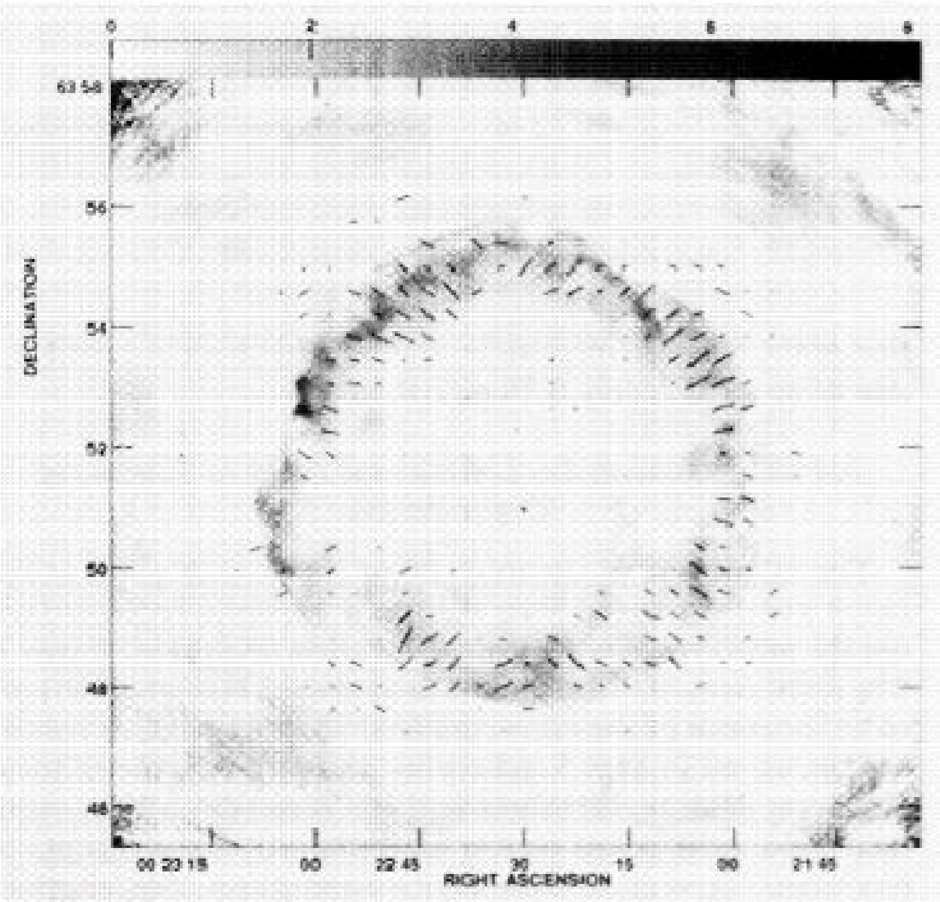

(b)

FIG. 5. Map of the remnant of Tycho's supernova showing local magnetic field organization and the direction of the mean local field averaged over boxes of various sizes, superposed on total intensity grey scale as shown in Dickel *et al.* 1991 (Paper I). The length of the vectors indicates the degree of organization in a box, and is proportional to Υ_{org}. The angle of the vector corresponds to the alignment of the mean magnetic field in a box. Positive values of the total intensity are represented with a peak of 8.1×10^{-3} Jy beam^{-1}; the grey scale is in units of 10^{-3} Jy beam^{-1}. (a) Box size of 30×30 pixels (0.55 pc$\times$0.55 pc). (b) Box size of 15×15 pixels (0.27 pc$\times$0.27 pc).

Dickel et al. 1991

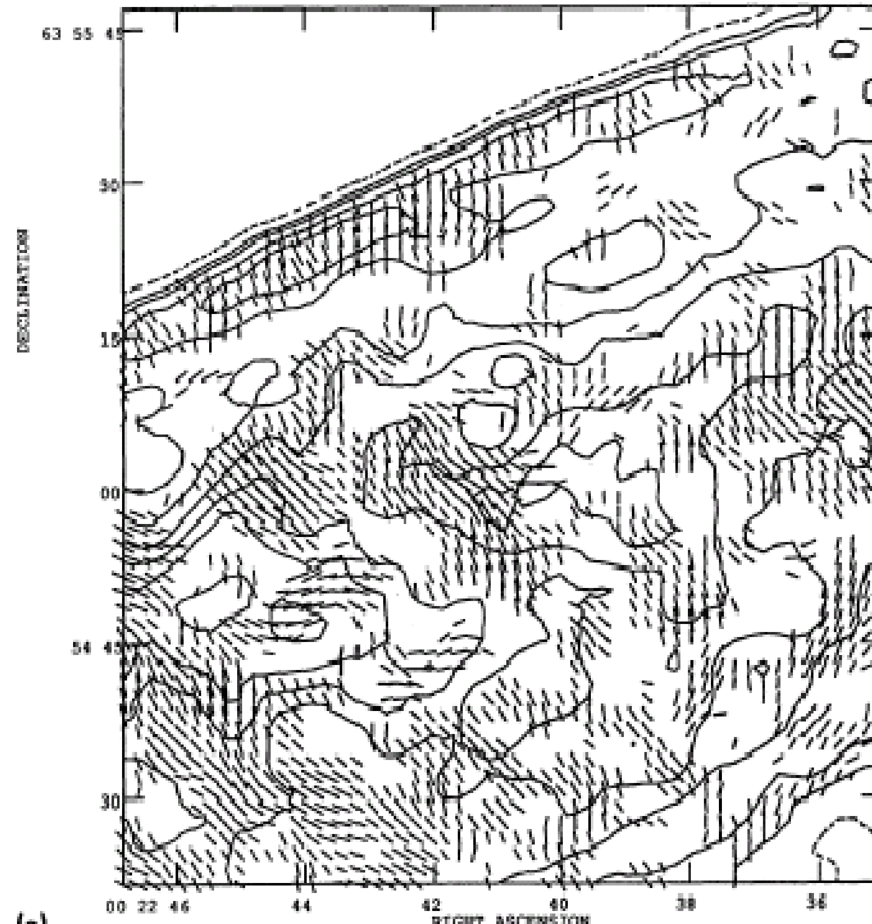

(a)

Radial magnetic fields were indeed observed in young SNRs

Schematic picture of the fast shock with accelerated particles

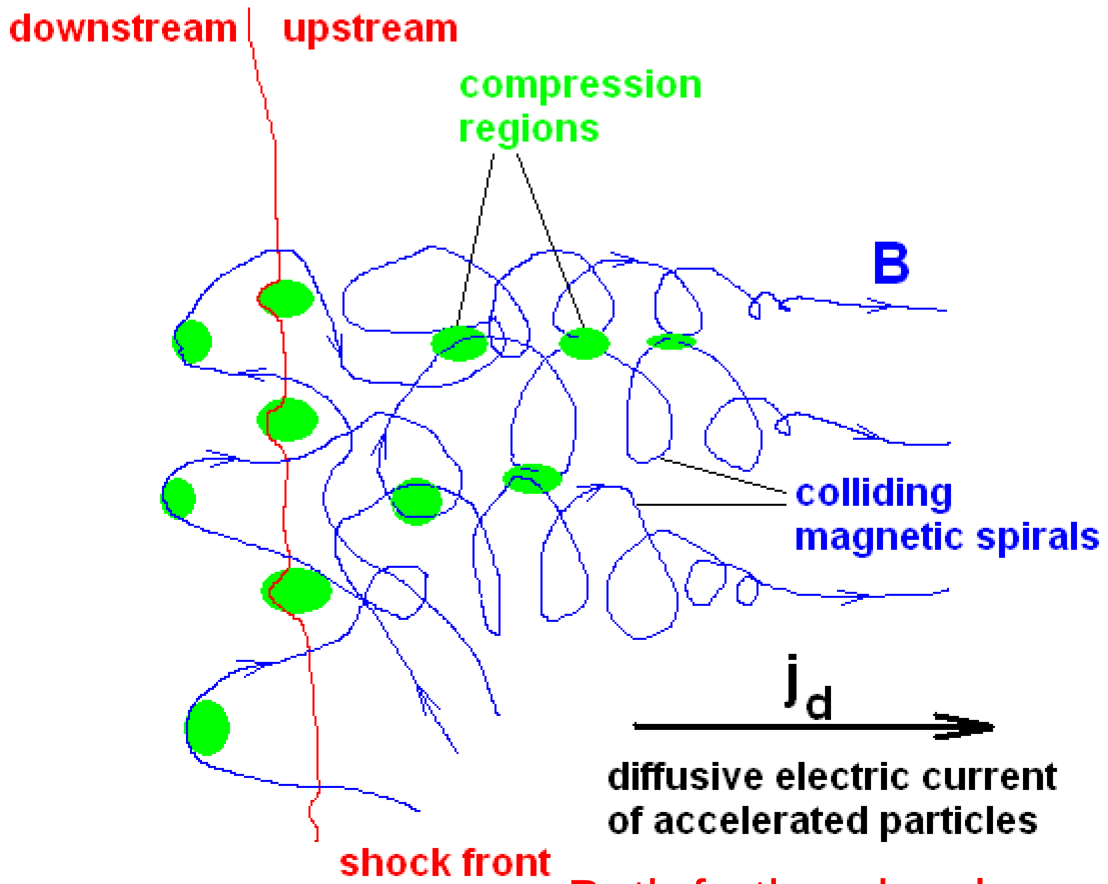

It is a great challenge - to perform the modeling of diffusive shock acceleration in such inhomogeneous and turbulent medium. Spectra of accelerated particles may differ from the spectra in the uniform medium.

Both further development of the DSA theory and the comparison with X-ray and gamma-ray observations are necessary

CR acceleration at the reverse shock (e.g.Ellison et al. 2005) ? Probably presents in Cas A (Helder & Vink 2008)

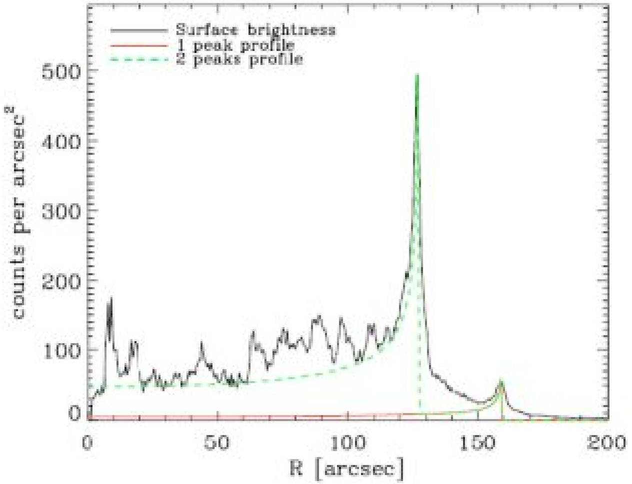

FIG. 3.— Radial surface brightness profile (smooth solid line) in the 4.2 to 6.0 keV energy band at an angle of 10° to 30° (including the featureless filament found by Hughes et al. (2000)). The smooth solid line indicates what the profile will look like if the surface brightness is produced by an emissivity function with only a peak at the outer shock. For the dashed line, we use an emissivity function with two peaks. Note that this is not a fit, just an illustrative example.

Magnetic field of ejecta?

B~R^{-2}, 10^4G at R=10^{13} cm -

10^{-8}G at R=10^{19}cm=3pc

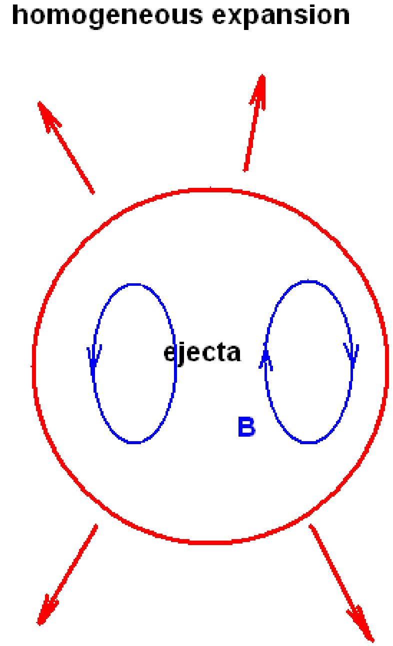

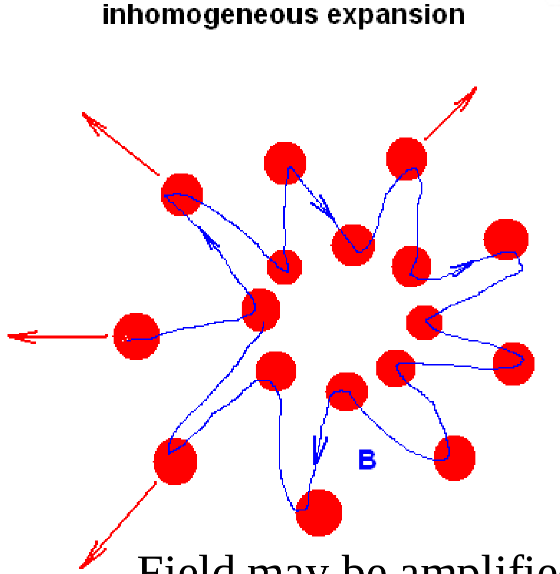

+additional amplification by the non-resonant streaming instability (Bell 2004)

Field may be amplified and become radial – enhanced ion injection at the reverse shock

Radio-image of Cas A

Atoyan et al. 2000

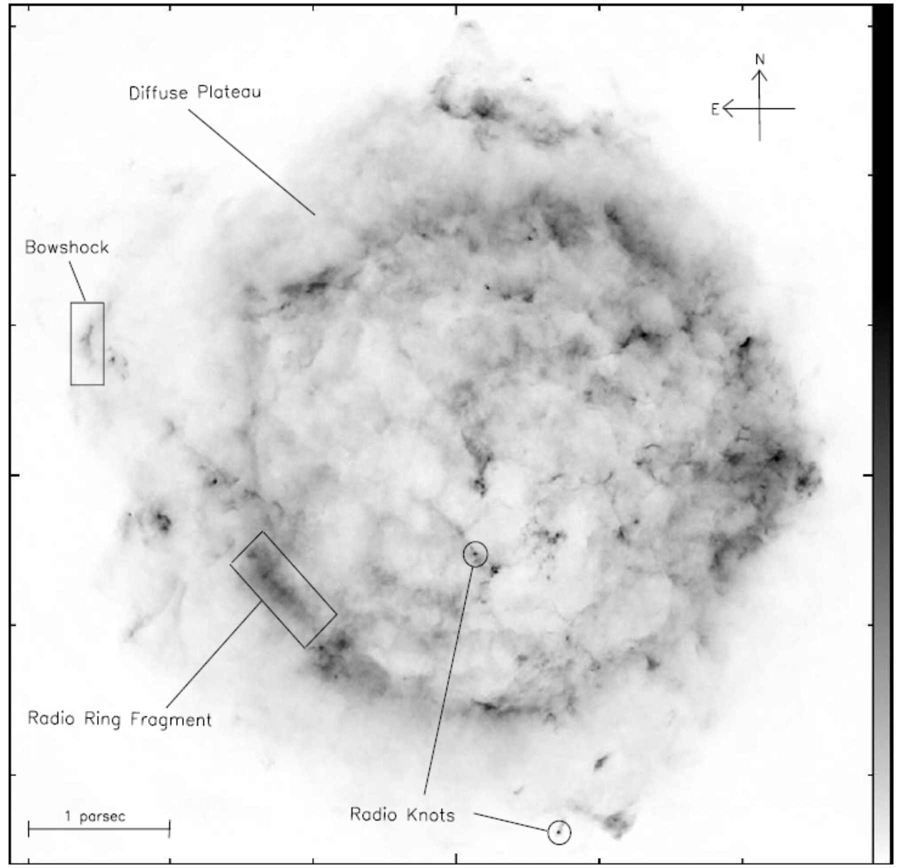

X-ray image of Cas A (Chandra)

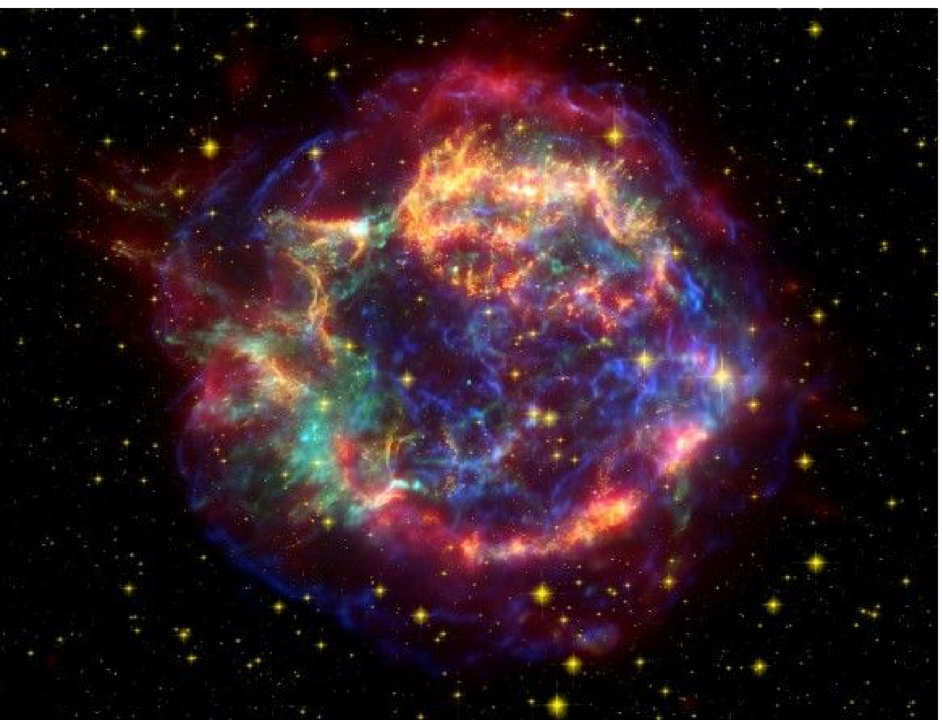

Inner bright radio- and X-ray-ring is related with the reverse shock of Cas A while the diffuse radio-plateau and thin outer X-ray filaments are produced by electrons accelerated at the forward shock.

Radio-image of RX J1713.7-3946 (Lazendic et al. 2004)

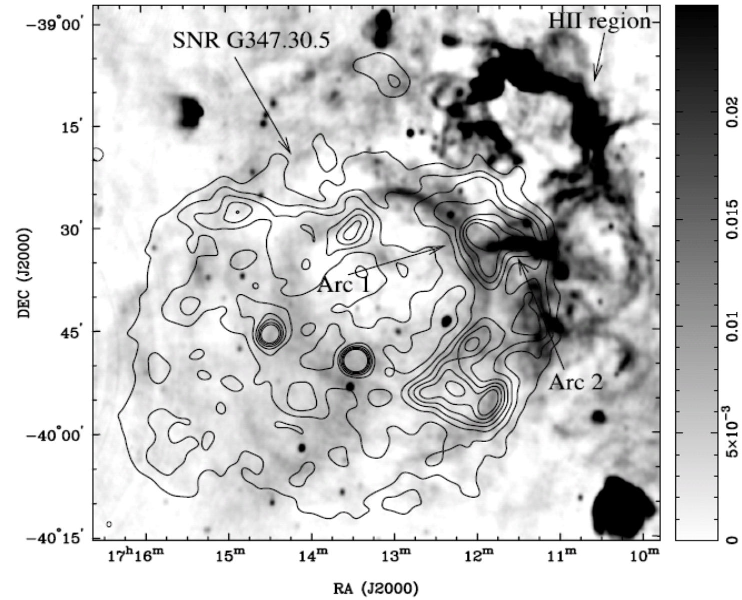

FIG. 5.—ATCA images of G347.3−0.5 and surrounding region at 1.4 GHz. The image was convolved with a Gaussian restoring beam of 46″ × 36″ (P.A. = −3.°8), shown by the tiny ellipse in the bottom left-hand corner. The image is overlaid with the *ROSAT* contours with the same levels as in Fig. 1. The linear gray scale is in units of Jy $beam^{-1}$.

X-rays: XMM-Newton, Acero et al. 2009

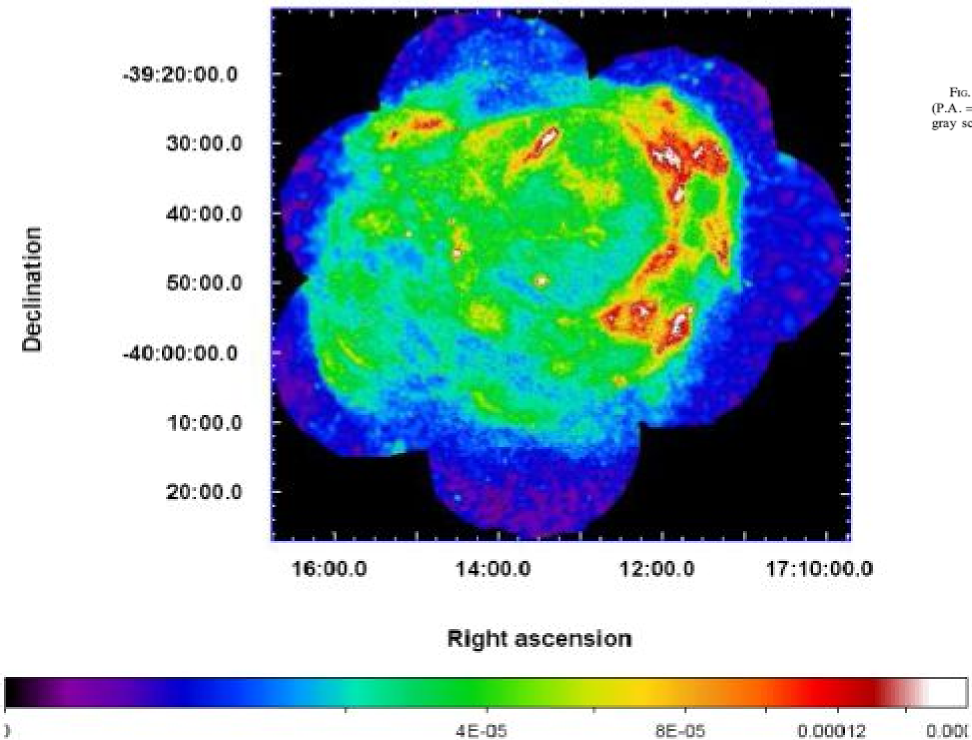

Fig. 1. EPIC MOS plus PN image in the 0.5-4.5 keV band. The units are $ph/cm^2/s/arcmin^2$ and the scale is square root. The image was adaptively smoothed to a signal-to-noise ratio of 10.

Inner ring of X-ray and radio-emission is probably related with electrons accelerated at the reverse shock.

Radioactivity and electron acceleration in SNRs

(Zirakashvili & Aharonian (2010), astro-ph:1011.4775)

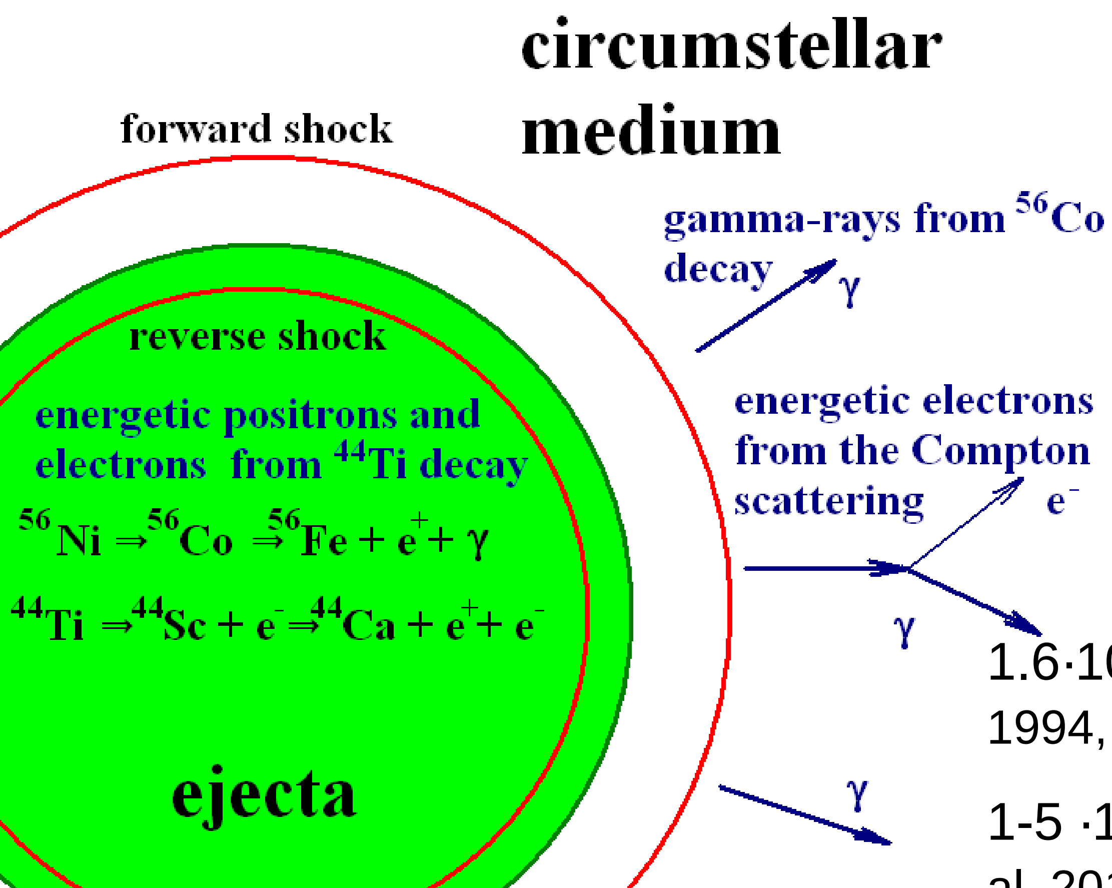

Forward and reverse shocks propagate in the medium with energetic electrons and positrons.

Cosmic ray positrons can be accelerated at reverse shocks of SNRs.

^{44}Ti $t_{1/2}$=63 yr

$1.6 \cdot 10^{-4}\ M_{sol}$ in Cas A, (Iyudin et al. 1994, Renaud et al. 2006)

$1\text{-}5 \cdot 10^{-5}\ M_{sol}$ in G1.9+0.3 (Borkowski et al. 2010)

“Radioactive” scenario in the youngest galactic SNR G1.9+0.3

X-ray image

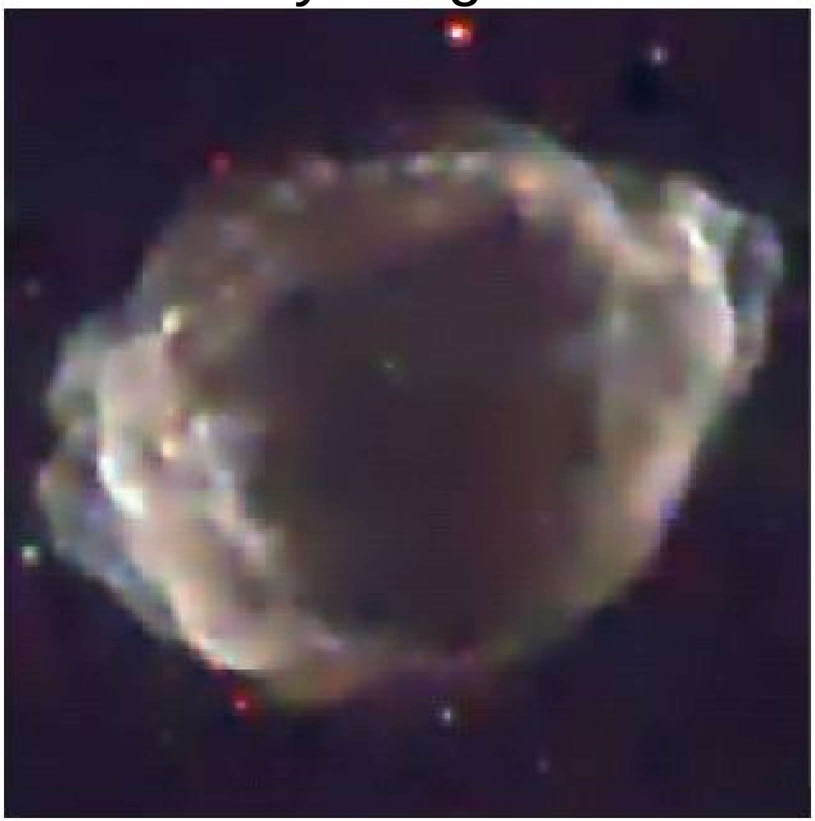

Figure 1. *Chandra* image of G1.9+0.3. Red, 1–3 keV; green, 3–4.5 keV; and blue, 4.5–7.5 keV. Image size is 127″ × 121″.

radio-image

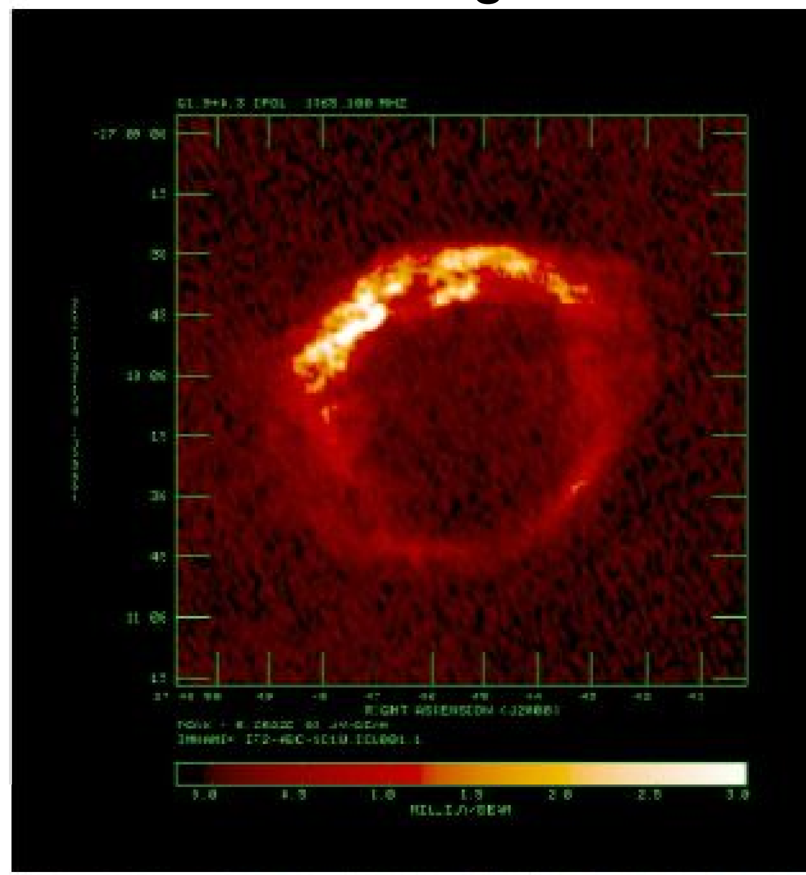

Thermal X-rays and 4.1 keV Sc line (product of ^{44}Ti) are observed from bright radio-regions (ejecta)

Borkowski et al. 2010

Numerical model of nonlinear diffusive shock acceleration

(Zirakashvili & Ptuskin 2011)

(natural development of existing models of Berezhko et al. (1994-2006), Kang & Jones 2006, see also half-analytical models of Blasi et al.(2005); Ellison et al. (2010))

$$\frac{\partial \rho}{\partial t} = -\frac{1}{r^2}\frac{\partial}{\partial r} r^2 u\rho \qquad (1)$$

$$\frac{\partial u}{\partial t} = -u\frac{\partial u}{\partial r} - \frac{1}{\rho}\left(\frac{\partial P_g}{\partial r} + \frac{\partial P_c}{\partial r}\right) \qquad (2)$$

$$\frac{\partial P_g}{\partial t} = -u\frac{\partial P_g}{\partial r} - \frac{\gamma_g P_g}{r^2}\frac{\partial r^2 u}{\partial r} - (\gamma_g - 1)(w - u)\frac{\partial P_c}{\partial r} \qquad (3)$$

$$\frac{\partial N}{\partial t} = \frac{1}{r^2}\frac{\partial}{\partial r} r^2 D(p,r,t)\frac{\partial N}{\partial r} - w\frac{\partial N}{\partial r} + \frac{\partial N}{\partial p}\frac{p}{3r^2}\frac{\partial r^2 w}{\partial r}$$

$$+\frac{\eta_f \delta(p - p_f)}{4\pi p_f^2 m}\rho(R_f + 0, t)(\dot{R}_f - u(R + 0, t))\delta(r - R_f(t))$$

$$+\frac{\eta_b \delta(p - p_b)}{4\pi p_b^2 m}\rho(R_b - 0, t)(u(R_b - 0, t) - \dot{R}_b)\delta(r - R_b(t)) \qquad (4)$$

Spherically symmetric HD equations + CR transport equation

Acceleration at forward and reverse shocks

Minimal electron heating by Coulomb collisions with thermal ions

Numerical results

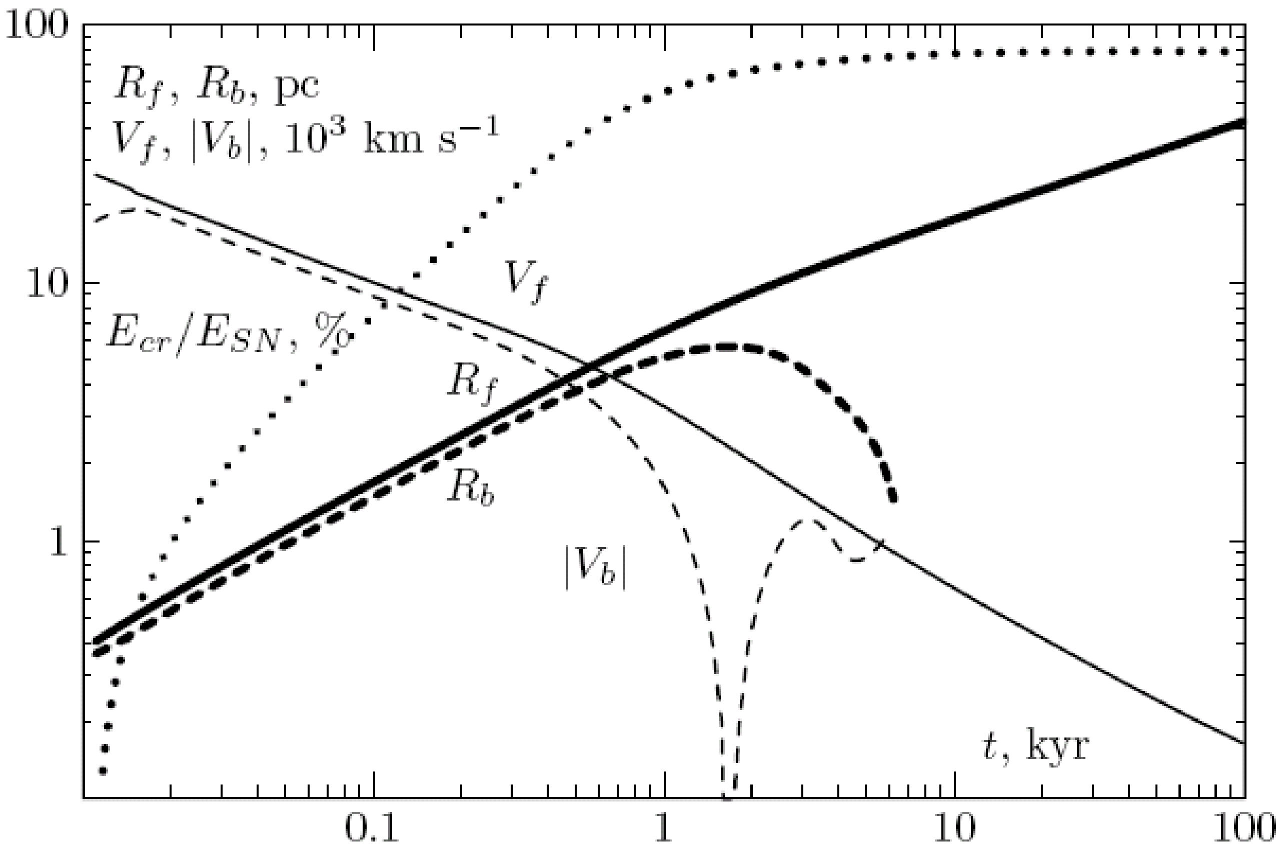

Figure 1: Dependencies on time of the forward shock radius R_f (thick solid line), the reverse shock radius R_b (thick dashed line), the forward shock velocity V_f (thin solid line) and the reverse shock velocity V_b (thin dashed line). The ratio of CR energy and energy of supernova explosion E_{cr}/E_{SN} (dotted line) is also shown.

$n_H = 0.1$ cm^{-3}

$B_0 = 5$ μG

$T = 10^4$ K

$\eta = 0.01$

Protons and electrons are injected at the forward shock, ions and positrons are injected at the reverse shock.

Magnetic amplification in young SNRs is taken into account

Radial profiles at T=1000 years

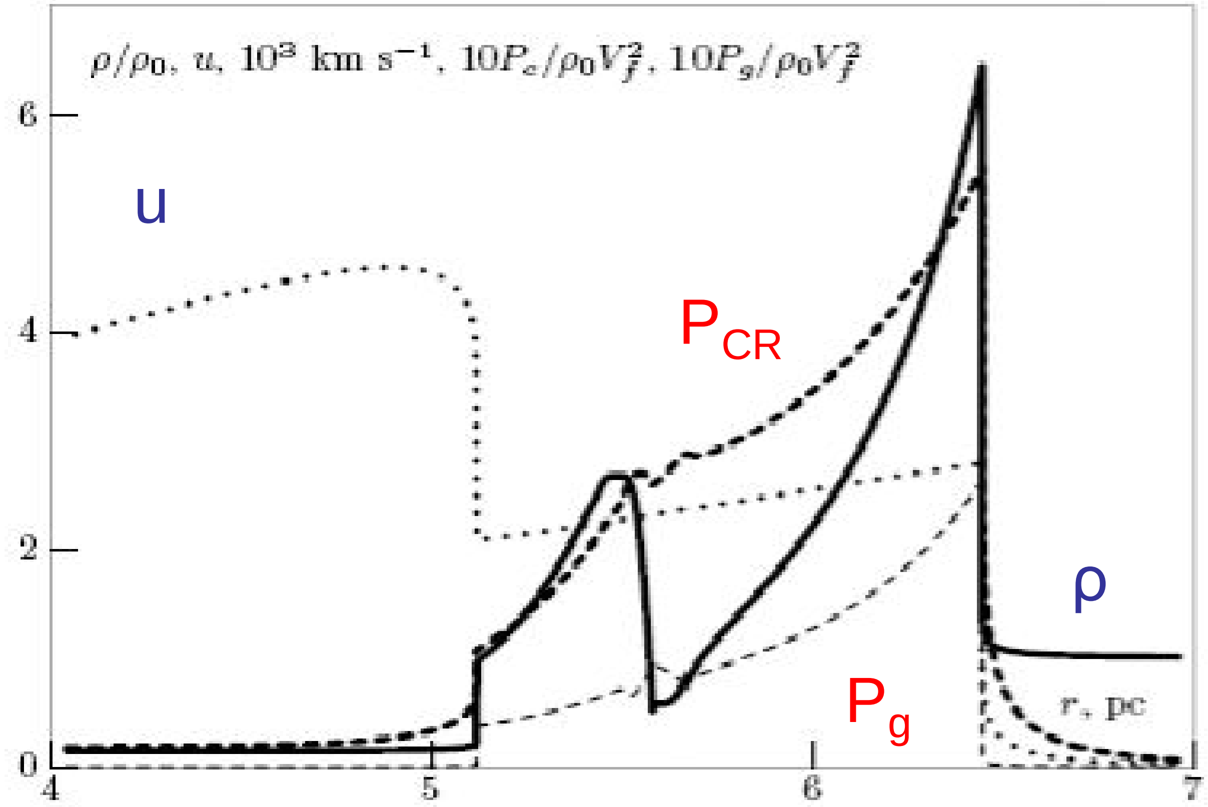

Figure 2: Radial dependencies of the gas density (thick solid line), the gas velocity (dotted line), CR pressure (thick dashed line) and the gas pressure (dashed line) at $t = 10^3$ yr. At this epoch the forward shock velocity is 3300 km s^{-1}, its radius is 6.5 pc, the reverse shock velocity is 1650 km s^{-1}, its radius is 5.1 pc, the magnetic field strength downstream of the forward shock is 160 μG while the magnetic field strength downstream the reverse shock is 56 μG.

Spectra of accelerated particles

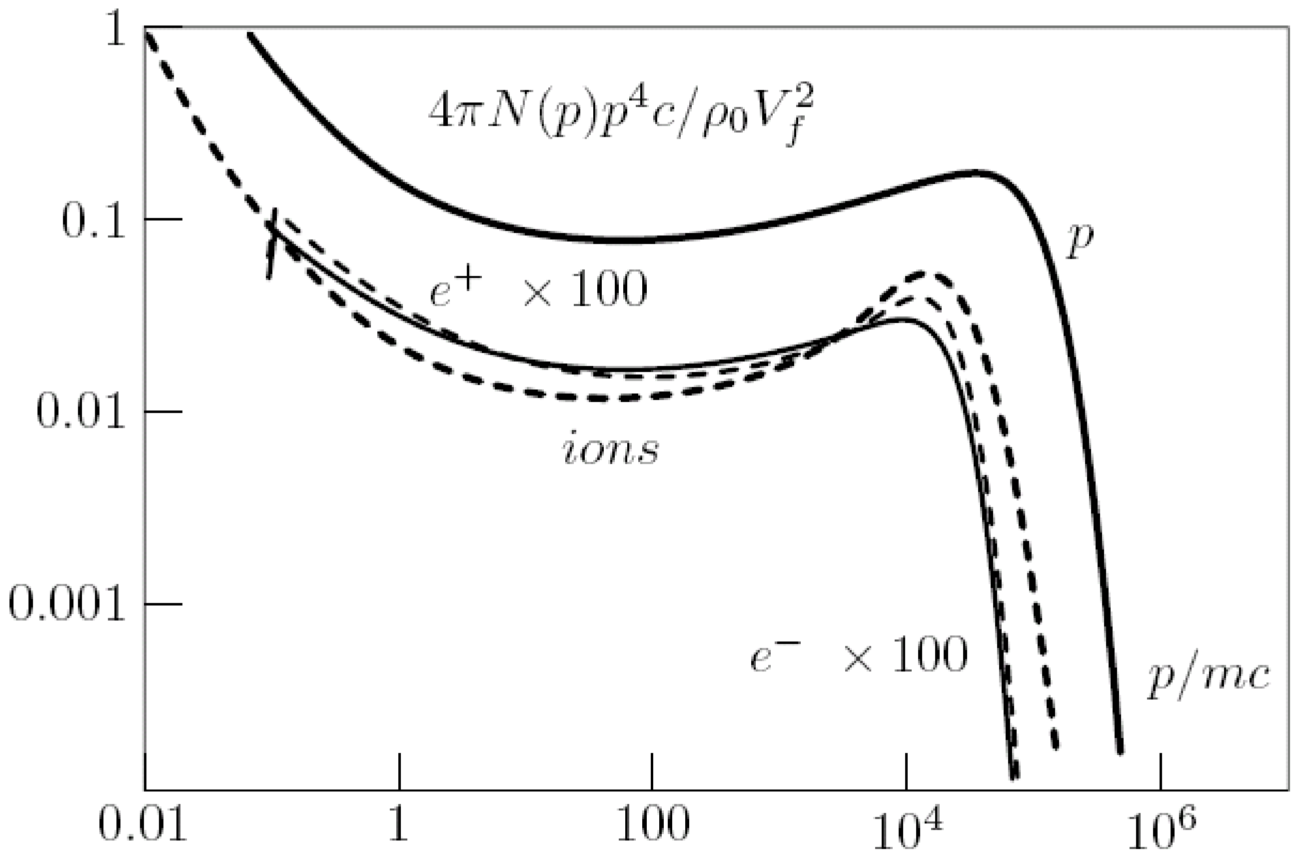

Figure 3: Spectra of accelerated particles at $t = 10^3$ yr. The proton spectrum at the forward shock (thick solid), ion spectrum at the reverse shock (thick dashed), electron spectrum at the forward shock (multiplied to the factor of 100, thin solid) and positron spectrum at the reverse shock (multiplied to the factor of 100, thin dashed) are shown. Spectrum of ions is shown as the function of momentum per nucleon and normalized to the baryonic number density.

Integrated spectra

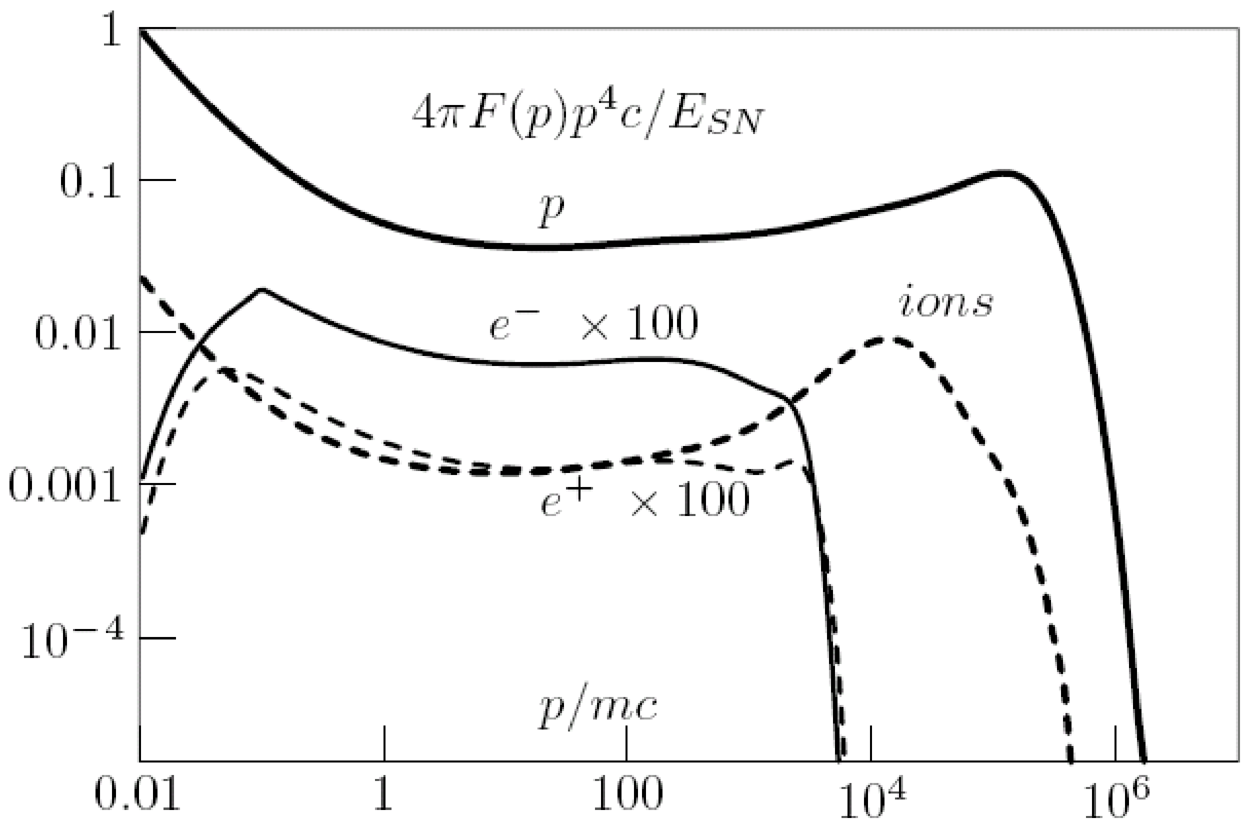

Figure 8: Spectra of particles produced in the supernova remnant during 10^5 yr. Spectrum of protons injected at the forward shock (thick solid line), spectrum of electrons injected at the forward shock (thin solid line), spectrum of ions injected at the reverse shock (thick dashed line) and the spectrum of positrons injected at the reverse shock (thin dashed line) are shown. Spectrum of ions is shown as the function of momentum per nucleon and normalized to the baryonic number density.

The input of the forward shock was considered earlier (Berezhko & Völk 2007, Ptuskin et al. 2010, Kang 2011)

Spectrum of ions is harder than the spectrum of protons because the ejecta density decreases in time.

Integrated spectra

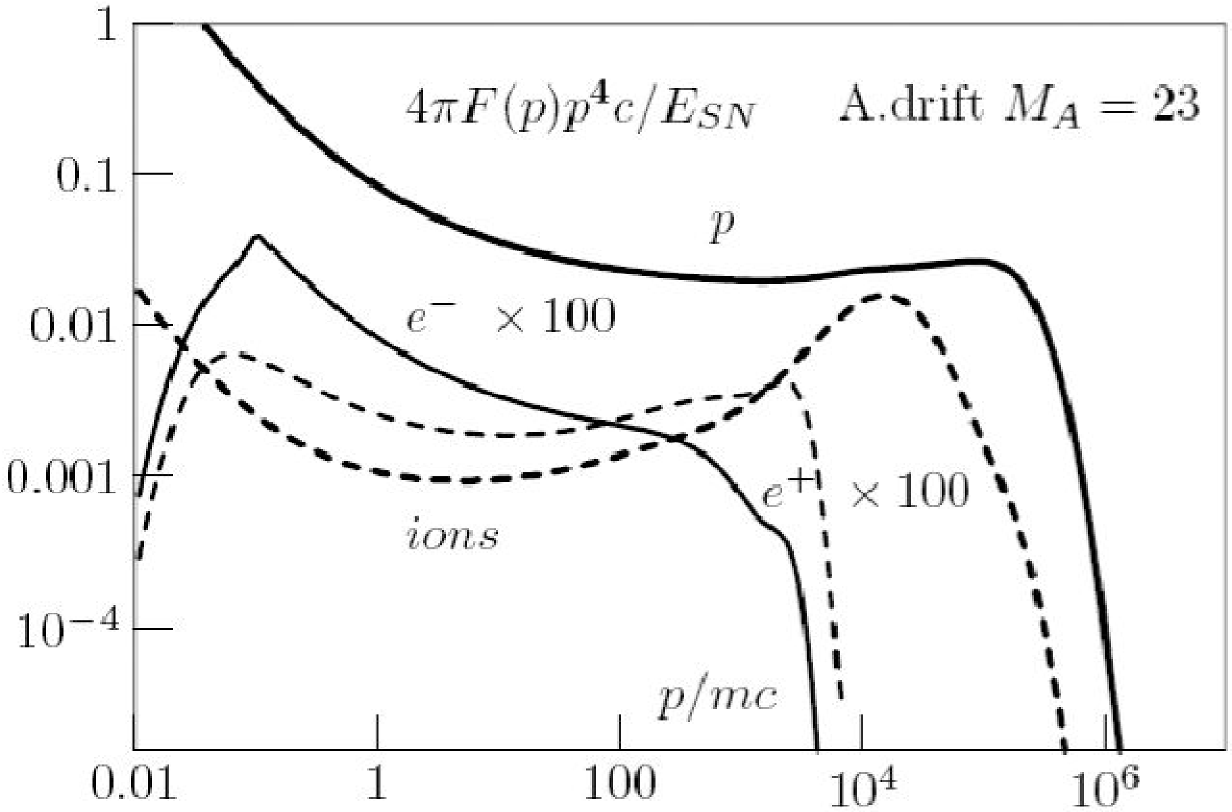

Figure 10: Spectra of particles produced in the supernova remnant during 10^5 yr in the model including the Alfvén drift downstream of the shocks. Spectrum of protons injected at forward shock (thick solid line), spectrum of electrons injected at the forward shock (thin solid line), spectrum of ions injected at the reverse shock (thick dashed line) and the spectrum of positrons injected at the reverse shock (thin dashed line) are shown. Spectrum of ions is shown as the function of momentum per nucleon and normalized to the baryonic number density.

Alfven drift downstream of the forward shock results in the steeper spectra of particles accelerated at the forward shock.

PAMELA results

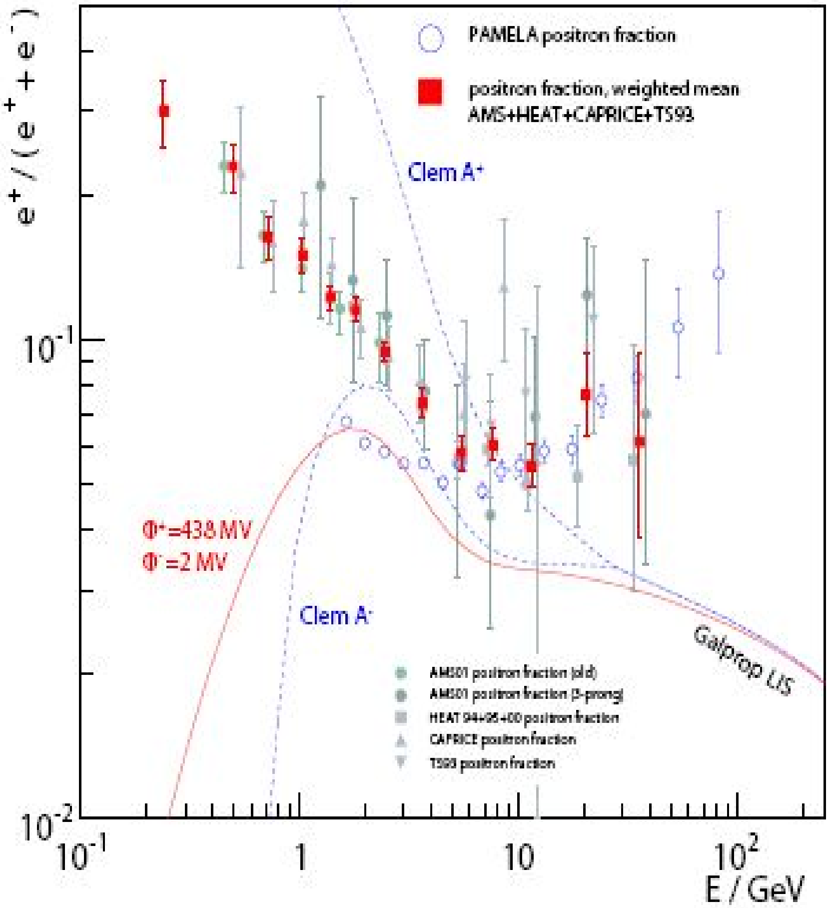

Fig. 1. Positron fraction data compared to predictions for the low-energy behaviour, based on the local interstellar spectrum (LIS) obtained in the conventional Galprop model. Data are from PAMELA [5], AMS-01 [3], [4], HEAT [2], CAPRICE [13] and TS-93 [14]. The weighted mean of the earlier measurements, taken during comparable solar conditions, is included for clarity. The solid line is based on charge-sign dependent modulation parameters in the force-field approximation formula (1), the dashed lines are obtained in the empirical model of Clem et al. [15], as described in the text.

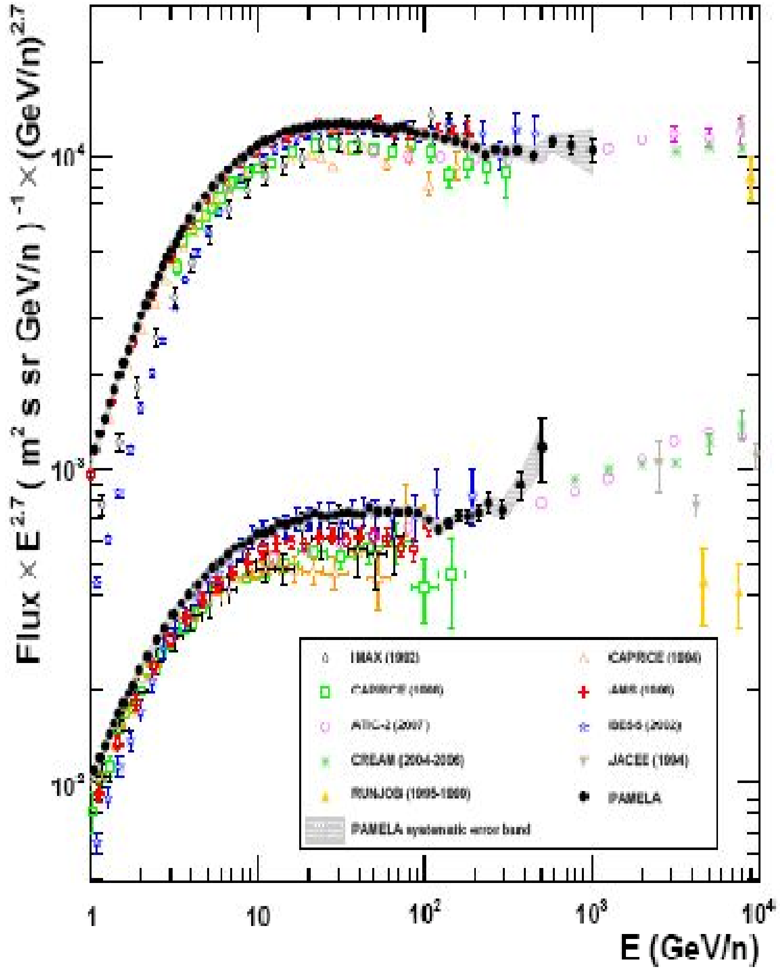

Proton and helium absolute fluxes measured by PAMELA above 1 GeV/n

Summary

1. Non-resonant streaming instability produced by the electric current of run-away CR particles results in the significant magnetic amplification at fast SNR shocks.
2. The perpendicular to the shock front component of the amplified magnetic field is larger than the parallel components downstream of the shock. This naturally explains the preferable radial orientation of magnetic fields in young SNRs.
3. The reverse shocks in SNRs can give a non-negligible output in to production of CR ions and positrons in comparison with the output of the forward shock.
4. Spectra of particles accelerated at the reverse shock can be harder than the spectra at the forward shock. This seems in agreement with the recent Pamela measurements of CR electron to positron ratio and harder observable spectra of CR nuclei.